Pergamon

Int. J. Heat Mass Transfer. Vol. 37, No. 12, pp. 1783–1793, 1994

0017–9310/94 $7.00 + 0.00

0017–9310(94)E0006–G

Unsteady mixed convection from a sphere in water-saturated porous media with variable surface temperature/heat flux

HOA D. NGUYEN and SEUNGHO PAIK
Idaho National Engineering Laboratory, P.O. Box 1625, Idaho Falls, ID 83415, U.S.A.

(*Received* 1 *June* 1993 *and in final form* 19 *November* 1993)

Abstract—Mixed convection about a sphere buried in a porous medium saturated with water is numerically investigated using a Chebyshev–Legendre spectral method. Both Darcy's law and the Boussinesq approximation together with effects due to nonlinear dependence of density on temperature are used to formulate the governing equations. Two types of surface condition are considered including variable surface temperature and surface heat flux which are modeled by Legendre expansions. Calculated results for the nonuniform heating and the nonuniform surface temperature cases demonstrate that the flow structures are not much different from the non-porous medium except for the recirculation zones which appear when the direction of the free stream velocity is opposite to the direction of the buoyancy force. Effects of nonuniform surface temperature are seen to dictate the heat flux distribution along the sphere surface and vice versa.

1. INTRODUCTION

TRANSFER processes involving porous materials occur in almost all engineering disciplines. Tien and Vafai [1] cited a number of specific examples ranging from natural processes to those of technological importance. Perhaps, one of the areas which has become the center of attention in recent years has been groundwater contamination in that pollutants enter the groundwater aquifer from the point of release by various mechanisms. Among the multitude of the underlying chemical and physical phenomena involved, advection is known to play a major role in contaminant transport and in some circumstances it is further augmented by buoyancy-induced convection. Such scenarios are typical in near-field modeling associated with hazardous waste repositories where the transport processes may be affected by the liberation of heat due to exothermic reactions of the emplaced wastes.

Over the years, studies of flow and transport associated with a body embedded in fluid-saturated porous media have concentrated on spheres, cylinders, and the like. Although geometrically simple, these configurations play an important role in practice and more importantly, they are instructional tools to deepen our understanding of the transport mechanisms which could be generalized to complex geometries. Of particular interest in this article is the sphere which seems, at least in certain aspects, to be somewhat lagging behind its cylindrical counterpart as far as theoretical development is concerned. Three types of solution have been reported for the natural convection problem about a sphere embedded within a saturated porous medium. At low and high Rayleigh numbers, the solutions have been obtained by regular perturbation method and boundary-layer analysis, respectively. For a more thorough review, readers are recommended to consult authorative books by Ene and Polisevski [2] and Nield and Bejan [3]. At intermediate Rayleigh numbers, available solutions were those of Pop and Ingham [4] who obtained the results via computer simulations based on a finite differencing scheme.

All of the accounts mentioned thus far assumed that the flow is driven by the buoyancy force which is a consequence of the density change. However, there exists a more general situation at which the thermally-induced flow field is superimposed on an external motion of the same order of magnitude; thereby neglecting one over the other would lead to erroneous results. Minkowycz *et al.* [5] and Cheng [6] have investigated this mixed convection problem on the basis of boundary layer approximations. Though useful in their own right, the boundary layer solutions have limited usefulness because they are only valid as long as thin boundary layers exist along the surface of the sphere. Because the boundary layer thickness grows as the inverse of the square root of the Rayleigh number, it becomes clear that the validity of these solutions does not extend to the cases when Rayleigh numbers are small. To the authors' knowledge, this situation has not been investigated.

Motivated by the lack of solutions to such an impor-

NOMENCLATURE

c	specific heat
B	buoyancy parameter
e	unit vector associated with spherical coordinates
g	gravity constant
$\hat{G}^{(1)}_{k,l}, \hat{G}^{(2)}_{k,l}$	Chebyshev matrix for first and second derivative respectively
H_{nk}	see equation (20)
K	permeability
NL	number of terms retained in the Legendre expansion
NT	number of collocation points less one
Nu	mean Nusselt number
p	fluid pressure
P_n	Legendre polynomial of order n
P_n^1	associated Legendre function
Pe	Peclet number
q	surface heat flux
$\bar{q}$	average surface heat flux
r	radial coordinate
R	sphere radius
Ra	Rayleigh number
S_{nk}	see equation (19)
t	time
T_i	Chebyshev polynomial of order i
u	velocity vector
Z	dimensionless temperature
$\tilde{Z}_{nk}$	expansion coefficient for temperature.

Greek symbols

α	thermal diffusivity
α^n_{ij}	see equation (22a)
β	isothermal expansion coefficient
γ^n_{ij}	see equation (22d)
δ_{ij}	Kronecker delta
θ	angular coordinate
κ	effective thermal conductivity
λ^n_{ij}	see equation (22c)
μ	viscosity
$\bar{\mu}$	$\cos\theta$
ξ	coordinate transformation, see equation (15b)
ρ	density
ϕ	porosity
Φ	see equation (7)
ψ	dimensionless stream function
$\tilde{\psi}_{nk}$	expansion coefficient for stream function
ω^n_{ij}	see equation (22b).

Superscript

m	time level.

Subscripts

f	pertains to fluid property
p	pertains to solid matrix
r	pertains to radial direction
s	pertains to sphere surface
θ	pertains to angular direction
∞	pertains to free stream condition.

tant problem, the present study is carried out to investigate the transient nature of the transport phenomena under conditions where boundary layer theory fails to capture the correct physics of the combined convection associated with a sphere embedded in fluid-saturated porous media. In a parallel effort, the present study also takes into account the effects due to density inversion of the working fluid. This characteristic is known to exist in water, especially near the freezing point.

2. FORMULATION

2.1. *Conceptual model*

The scenario considered consists of a solid sphere of radius R embedded in an unbounded porous medium characterized by a porosity ϕ and a permeability K (Fig. 1). Initially, the sphere is at the same temperature as the ambience where a pre-existing flow of velocity U_∞ is experienced. Suddenly, the sphere acquires a higher temperature; thus creating a heat flow from the particle to the surrounding porous medium in accordance with the second law of thermodynamics. As a result of the absorption of energy, fluid particles in the proximity of the hot sphere become warmer, causing a density variation which subsequently generates a motion in the direction opposite to gravity. This gravity-induced flow when superimposed on the pre-existing motion would modify the flow field and hence the temperature field. Depending on the direction of the free stream velocity and buoyancy, this forcing mechanism could aid or oppose the main flow and could produce dominant effects on heat transfer.

In view of the complexities in the present investigation, we shall formulate the problem with the following assumptions: (i) the porous medium is rigid

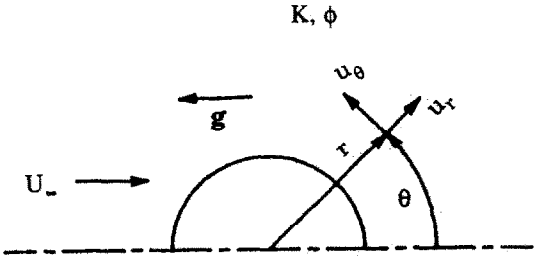

FIG. 1. Schematic of the physical system.

and nondeformable with uniform hydraulic properties, (ii) the fluid is Newtonian with constant properties except density which varies as a direct consequence of change in temperature, (iii) the transport processes are axisymmetric with the flow obeying Darcy's law, (iv) the Boussinesq approximation is valid with a parabolic density–temperaure relationship, and (v) the solid matrix and the fluid are in local thermodynamic equilibrium which is justifiable in view of the large surface area available for heat transfer.

2.2. *Governing equations*

As usual, the heat transfer process associated with the sphere is governed by the conservation of mass, momentum, and energy. Under the assumptions stated above, these laws, when applied to a differential control volume, result in the following equations expressed in vector notation as

$$\nabla \cdot \mathbf{u} = 0, \tag{1}$$

$$[\phi(\rho c)_f + (1+\phi)(\rho c)_p]\frac{\partial Z}{\partial t} + (\rho c)_f \mathbf{u}\cdot\nabla Z = \nabla\cdot(\kappa\nabla Z), \tag{2}$$

$$\mathbf{u} = -\frac{K}{\mu}\{\nabla p + \rho g \beta (Z - Z_\infty)^2\}, \tag{3}$$

in which equation (3) reflects the use of the Boussinesq approximations which assume constant density everywhere except in the gravity term where the density–temperature relationship has been modeled by a quadratic formula [7, 8]. In the above equations, c is the sensible heat, $\mathbf{g}$ is the gravity vector, K is the permeability, p is the pressure, t is the time, $\mathbf{u}$ is the Darcy velocity vector, Z is the temperature, β is the thermal expansion coefficient, κ is the effective thermal conductivity, μ is the dynamic viscosity, ρ is the density, and ϕ is the porosity. Regarding the effective conductivity of the porous medium, several analytical as well as empirical models have been proposed, but the weighted geometric mean has been recommended for practical purposes [3].

For the problem under consideration, it is more convenient to recast equations (1)–(3) in term of the stream function which is related to the velocity by

$$\mathbf{u} = \frac{\mathbf{e}_r}{r^2 \sin\theta}\frac{\partial \Psi}{\partial \theta} - \frac{\mathbf{e}_\theta}{r\sin\theta}\frac{\partial \Psi}{\partial r}; \tag{4}$$

thereby resulting in

$$\frac{1}{\sin\theta}\frac{\partial^2 \Psi}{\partial r^2} + \frac{1}{r^2}\frac{\partial}{\partial\theta}\left(\frac{1}{\sin\theta}\frac{\partial \Psi}{\partial \theta}\right) = B\left[r\sin\theta Z\frac{\partial Z}{\partial r} + \cos\theta Z\frac{\partial Z}{\partial \theta}\right], \tag{5}$$

$$\Phi\frac{\partial Z}{\partial t} - \frac{1}{r^2\sin\theta}\frac{\partial(\Psi, Z)}{\partial(r,\theta)} = \frac{2}{Pe}\left[\frac{1}{r^2}\frac{\partial}{\partial r}\left(r^2\frac{\partial Z}{\partial r}\right) + \frac{1}{r^2\sin\theta}\frac{\partial}{\partial\theta}\left(\sin\theta\frac{\partial Z}{\partial\theta}\right)\right], \tag{6}$$

where we have employed $\partial(,)/\partial(,)$ to denote the Jacobian. In these equations, all the variables have been made dimensionless by introducing the following nondimensional quantities:

$$\left.\begin{aligned} r' &= \frac{r}{R}, \quad t' = \frac{tU_\infty}{R}, \\ Z' &= \frac{Z - Z_\infty}{Z_s - Z_\infty}, \quad \Psi' = \frac{\Psi}{R^2 U_\infty}, \\ \mathbf{u}' &= \frac{\mathbf{u}}{U_\infty}, \quad \Phi = \frac{\phi(\rho c)_f + (1-\phi)(\rho c)_p}{(\rho c)_f}, \\ Pe &= \frac{2U_\infty R}{\alpha}, \quad B = \frac{2\rho g \beta K R (Z_0 - Z_\infty)^2}{\mu U_\infty} \end{aligned}\right\} \tag{7a}$$

for the nonuniform surface temperature case. These definitions are also extended to the variable surface heat flux case with the exception of Z' and B which now take the forms

$$Z' = \frac{(Z - Z_\infty)\kappa}{qR}, \quad B = \frac{2\rho g \beta K R^3 q^2}{\mu \kappa^2}. \tag{7b}$$

Note that a prime has been used to indicate dimensionless variables; however, it has been dropped in equations (5) and (6) for convenience. These equations are subjected to the following boundary conditions.

I. Axisymmetry: at the axis of symmetry, the mathematical constraints are

$$\Psi(t, r, 0) = \Psi(t, r, \pi) = 0, \tag{8}$$

$$Z(t, r, 0) = Z(t, r, \pi) = 0. \tag{9}$$

II. Far-field: the stream function and temperature approach the free-stream values in an asymptotic manner, i.e.

$$\lim_{r\to\infty} \Psi(t, r, \theta) \to \frac{r^2}{2}\sin^2\theta, \tag{10}$$

$$\lim_{r\to\infty} Z(t, r, \theta) \to 0. \tag{11}$$

III. Sphere surface: the necessary requirements include no-slip condition and the continuity of temperature/heat flux. These lead to the following constraints:

$$\Psi(t, 1, \theta) = 0, \tag{12}$$

$$\begin{cases} Z(t, 1, \theta) = \sum_{n=0}^{\infty} a_n P_n(\cos\theta) \\ \quad \text{for nonuniform surface temperature} \\ -\dfrac{\partial Z}{\partial r}(t, 1, \theta) = \sum_{n=0}^{\infty} a_n P_n(\cos\theta) \\ \quad \text{for nonuniform heating} \end{cases} \tag{13a, b}$$

where we have expanded the nonuniform surface quantities (13a, b) in the form of the Legendre series. From the numerical standpoint, several types of interpolation functions are possible for representing the surface temperature/heat flux; however, the Legendre functions are selected in order to be consistent with the temperature expansion to be proposed in the next section.

To complete the problem specification, the initial conditions are prescribed such that the fluid is motionless and the sphere is at the ambient temperature. These are

$$\Psi(0, r, \phi) = 0, \quad Z(0, r, \theta) = 0. \tag{14}$$

In what follows, a hybrid numerical method that combines various approaches of weighted residual principles is described for transforming the governing differential equations to an algebraic system. From this, a computer code is developed for performing parametric studies to uncover the nature of mixed convection in porous media.

3. METHOD OF SOLUTION

As pointed out by Pop and Ingham [4] in their study of natural convection about a sphere embedded in a saturated porous medium, the unboundedness of the flow domain and the far-field boundary condition for the stream function necessitate special attention and must be resolved before numerical computations can proceed. While the former can easily be eliminated by a domain truncation or a coordinate transformation, the latter can be alleviated by working with a pseudo-stream function to be defined shortly. Considering these potential difficulties, we adopt the following change of variables:

$$\psi = \frac{\Psi}{r^2}, \quad \bar{\mu} = \cos\theta, \quad \xi = 1 - \frac{2}{r} \tag{15a, b, c}$$

so that the deployment of the mapping (15c) allows the grid points to be accumulated near the sphere surface. Such a gridding is very preferable for resolving stiff gradients which are expected to exist as convection becomes dominant.

Following an earlier work on spectral methods [9], the dependent variables ψ and Z are expanded as series of products of Legendre, $P_n(\bar{\mu})$, and Chebyshev, $T_k(\xi)$, polynomials, i.e.

$$\psi = \sum_{n=1}^{\infty} \sum_{k=0}^{\infty} \tilde{\psi}_{nk}(t) T_k(\xi) \int_{\bar{\mu}}^{1} P_n(\bar{\mu})\, \mathrm{d}\bar{\mu}, \tag{16a}$$

$$Z = \sum_{n=0}^{\infty} \sum_{k=0}^{\infty} \tilde{Z}_{nk}(t) T_k(\xi) P_n(\bar{\mu}) \tag{16b}$$

in which $\tilde{\psi}_{nk}$s and $\tilde{Z}_{nk}$s are the spectral coefficients of the corresponding dependent variable being expanded and are functions of time only.

By substituting equations (16a, b) into equations (5) and (6), then making use of the orthogonal properties and recursive formulas of Legendre functions, the equations become free of angular dependence. Next, the weighted residual principles can be applied to further simplify the resulting equations via forcing them to be error-free at the Gauss–Lobatto points, herein referred to as the collocation points. Thus,

$$\sum_{k'=0}^{NT} \{(1-\xi_k)^2 \hat{G}^{(2)}_{kk'} + 2(1-\xi_k)\hat{G}^{(1)}_{kk'}\}\psi_{nk'} - (n+2)(n-1)\psi_{nk} = S_{nk}, \tag{17}$$

$$\Phi \frac{\mathrm{d}Z_{nk}}{\mathrm{d}t} - \frac{1}{2Pe}\left\{(1-\xi_k)^4 \sum_{k'=0}^{NT} \hat{G}^{(2)}_{kk'} Z_{nk'} - n(n+1)(1-\xi_k)^2 Z_{nk}\right\} = H_{nk}, \tag{18}$$

where the spectral coefficients have been eliminated in favor of the physical variables by means of an inverse transform so that the computations can be carried out in the physical space. Note that we have truncated the series in (16a, b) at NT for the inner summation and NL for the outer summation and have used $\hat{G}^{(l)}_{k,j}$ to represent the $(NT+1)\times(NT+1)$ lth Chebyshev derivative matrix. Because closed form expressions for the entries of the Chebyshev derivative matrix have been given elsewhere [10], they are omitted here.

Equations (17) and (18) constitute a system of algebraic differential equations that can be solved by numerous techniques. Of particular interest in this work is the combined Adams–Bashforth and the backward Euler formulas commonly used for integrating the convection and diffusion terms of equation (18), respectively. Upon applying, one arrives at

$$\frac{\Phi}{\Delta t(1-\xi_k)^2} Z^{m+1}_{nk} - \frac{1}{2Pe}\left\{(1-\xi_k)^2 \sum_{k'=0}^{NT} \hat{G}^{(2)}_{kk'} Z^{m+1}_{nk'} - n(n+1) Z^{m+1}_{nk}\right\} = \frac{\Phi}{\Delta t(1-\xi_k)^2} Z^{m}_{nk} + \frac{1}{2(1-\xi_k)^2}[3H^{m}_{nk} - H^{m-1}_{nk}], \tag{19}$$

where the superscript m denotes the time level and Δt is the time increment. Despite the Adams–Bashforth scheme being second-order accurate in time, the overall accuracy of equation (19) is first order. Owing to the explicit treatment of the convection term, the momentum–energy couplings become one-way and can be completely removed by first solving the temperature field, then the velocity field.

The short-hand notations, S_{nk} and H_{nk}, employed to abbreviate the convection terms in the above equations may be given explicitly by

$$S_{nk} = B \sum_{i=0}^{NL} \sum_{j=0}^{NL} \times \left\{ \alpha_{ij}^{n} (1-\xi_k) Z_{jk} \sum_{k'=0}^{NT} \hat{G}_{kk'}^{(1)} Z_{ik'} - \omega_{ij}^{n} Z_{ik} Z_{jk} \right\}, \quad (20)$$

$$H_{nk} = -\tfrac{1}{2}(1-\xi_k)^2 \sum_{i=0}^{NL} \sum_{j=1}^{NL} \times \left\{ \lambda_{ij}^{n} \psi_{jk} \sum_{k'=0}^{NT} \hat{G}_{kk'}^{(1)} Z_{ik'} + \gamma_{ij}^{n} Z_{ik} \times \left(\sum_{k'=0}^{NT} \hat{G}_{kk'}^{(1)} \psi_{jk'} + \frac{2}{(1-\xi_k)} \psi_{jk} \right) \right\} \quad (21)$$

with the coefficients $\alpha_{ij}^{n}, \omega_{ij}^{n}, \lambda_{ij}^{n}$, and γ_{ij}^{n} given by

$$\alpha_{ij}^{n} = \frac{2n+1}{2} \int_{-1}^{1} P_i P_j P_1^1 P_n^1 \, \mathrm{d}\bar{\mu}, \quad (22a)$$

$$\omega_{ij}^{n} = \frac{2n+1}{2} \int_{-1}^{1} P_i^1 P_j P_1 P_n^1 \, \mathrm{d}\bar{\mu}, \quad (22b)$$

$$\lambda_{ij}^{n} = \frac{2n+1}{2} \int_{-1}^{1} P_i P_j P_n \, \mathrm{d}\bar{\mu}, \quad (22c)$$

$$\gamma_{ij}^{n} = \frac{(2n+1)}{2j(j+1)} \int_{-1}^{1} P_i^1 P_j^1 P_n \, \mathrm{d}\bar{\mu}, \quad (22d)$$

which can efficiently be evaluated by means of a Gaussian quadrature formula. Alternatively, these integrals can be expressed in terms of '3-J' symbols as normally done in mathematical literature and details to compute them can be found in the monograph by Rottenberg *et al.* [11].

4. PHYSICAL QUANTITIES

One of the important parameters in heat transfer analysis is the normalized surface heat flux q computed from the following expression:

$$q(t,\bar{\mu}) = -2\left(\frac{\partial Z}{\partial \xi}\right)_{\xi=-1} = -2 \sum_{n=0}^{NL} \sum_{k'=0}^{NT} \hat{G}_{NTk'}^{(1)} Z_{nk'}(t) P_n(\bar{\mu}). \quad (23)$$

Traditionally, this quantity is reported in the form of the mean Nusselt number which, by definition, is obtained by averaging the local heat flux over the entire surface area of the sphere. Upon performing the necessary operations and making use of the orthogonal property of the Legendre function, the mean Nusselt number based on the sphere diameter becomes

$$Nu(t) = -4 \sum_{k'=0}^{NT} \hat{G}_{NTk'}^{(1)} Z_{0k'}(t) \quad (24)$$

in that all terms drop out except the zeroth term. In the case of the specified surface heat flux, the appropriate quantity of interest is the surface temperature which can be calculated from

$$Z_s(t,\bar{\mu}) = \sum_{n=1}^{NL} Z_{nNT} P_n(\bar{\mu}). \quad (25)$$

In subsequent discussion, the heat transfer process will be examined in greater detail, and the quantities derived in this section will be used to assist in interpreting the simulation results.

Table 1. Summary of simulation parameters.

Parameter	Value
NL	12
NT	100
Φ	1.43
Δt	10^{-3}

5. RESULTS AND DISCUSSION

Before going into the main focus of this section, we summarize the simulation parameters. In Table 1, the truncation parameters were chosen on the basis of our past experience gained in a similar study [12] where convergence has been confirmed. Thus, those values were again adopted for the range of the Peclet number and the buoyancy parameter investigated in the present study without re-examining the matter. For the purpose of illustrating the physical insight, the remaining discussion will be organized into two separate sub-sections. Each is devoted to a specific type of surface boundary condition described in the Formulation and is accompanied by a parametric study with Pe and B varying.

5.1. *Nonuniform surface temperature*

We now look into the temporal development of the flow and temperature fields as we keep Pe at 10 while B is altered to represent pure forced convection ($B = 0$), and combined convection with gravity acting in either the same or opposite direction as the free stream velocity ($B = -10, 10$). Also, the surface temperature in these three cases is taken to be uniform with $a_0 = 1$. Unless otherwise indicated, the heat capacity ratio Φ is assumed to have a value of 1.43. Figures 2–4 illustrate how the velocity and temperature fields evolve in time as depicted at three different instances to show the early, intermediate, and late periods. For $B = 0$ (Fig. 2), the velocity field is invariant with respect to time whereas the temperature field evolves in a similar fashion as that encountered in a non-porous medium with the same physical setting. That is, the early stage of its development is controlled by the conductive mechanism whose dominant role diminishes in favor of the convection as time progresses, thereby leading to asymmetric temperature contours. In Fig. 3, buoyancy is allowed to take place and act in the direction of the free stream velocity. Here, it is easy to notice a drastic change

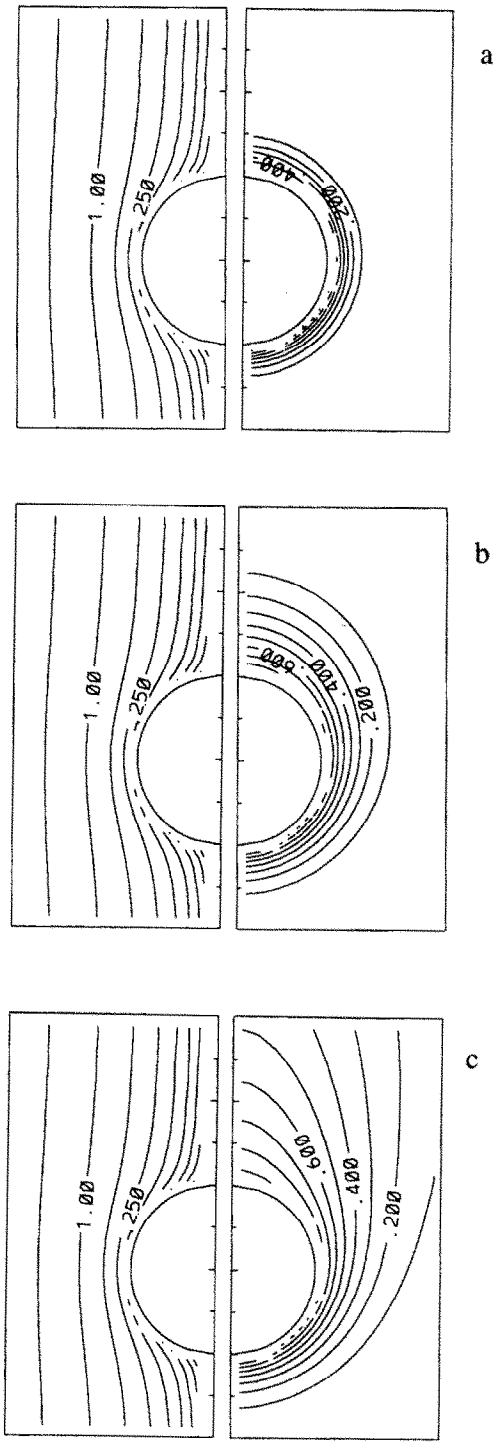

FIG. 2. Streamlines and isotherms for $Pe = 10$, $B = 0$. (a) $t = 0.2$, (b) $t = 1$, (c) $t = 8.6$.

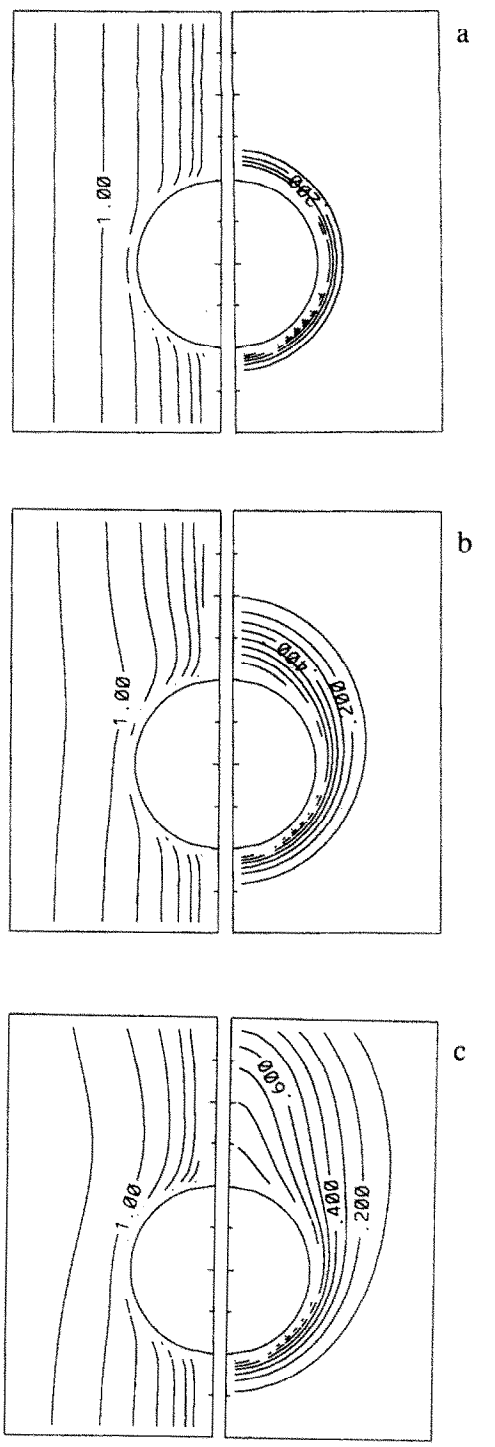

FIG. 3. Streamlines and isotherms for $Pe = 10$, $B = 10$. (a) $t = 0.1$, (b) $t = 0.5$, (c) $t = 1.8$.

of the streamline levels implying a considerable flow enhancement of the fluid particles in the vicinity of the sphere. Such a behavior is attributed to the aid of the motion generated by density difference. In addition to that, the flow pattern appears to be somewhat deflected downstream. Due to the aid of the buoyancy-generated motion, the isotherms are further elongated in the streamwise direction when the temperature contours in Figs. 2 and 3 are compared. Figure 4 illustrates the velocity and temperature distributions under the same circumstance as in Fig. 3 except for the direction of gravity which is now in the reversed direction. In this case, the buoyancy force produces a flow current against the free stream, thus

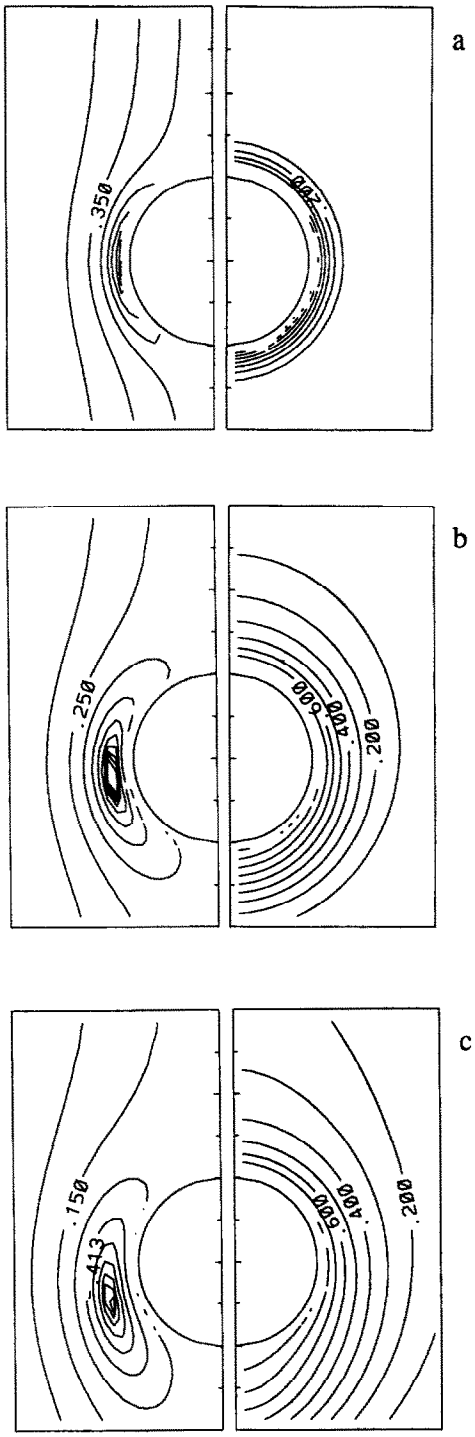

FIG. 4. Streamlines and isotherms for $Pe = 10$, $B = -10$. (a) $t = 0.2$, (b) $t = 2$, (c) $t = 12.2$.

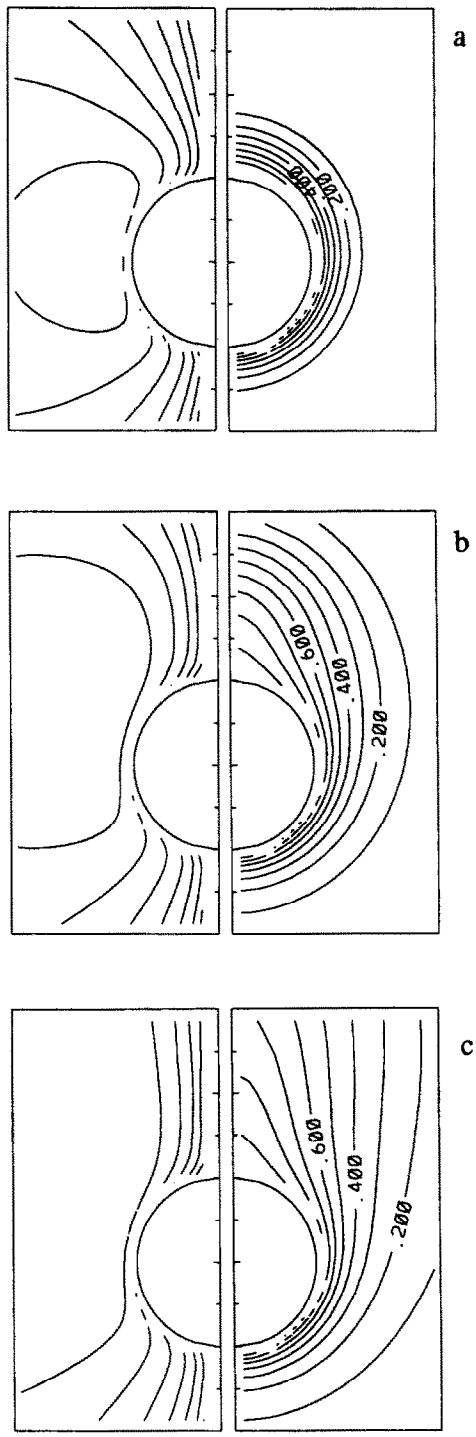

FIG. 5. Streamlines and isotherms for $Pe = 2$, $B = 50$. (a) $t = 0.1$, (b) $t = 0.5$, (c) $t = 1.8$.

causing a significant change in the flow structure. It is the existence of the circulation zones on the upper and lower surface of the sphere that modifies the flow and they are triggered at a very early time and keep growing thereafter until the time-invariant state is fully established. As a first attempt to verify the results presented thus far, the flow and temperature fields given in Fig. 5 for the case of pure natural convection with $B = 50$ are now compared with the existing solution. Even though the flow develops in a different fashion, the temperature is quite similar to those in Figs. 2 and 3 as one would expect. At steady-state ($t = 1.8$), the predicted streamlines agree qualitatively well with Pop and Ingham [4].

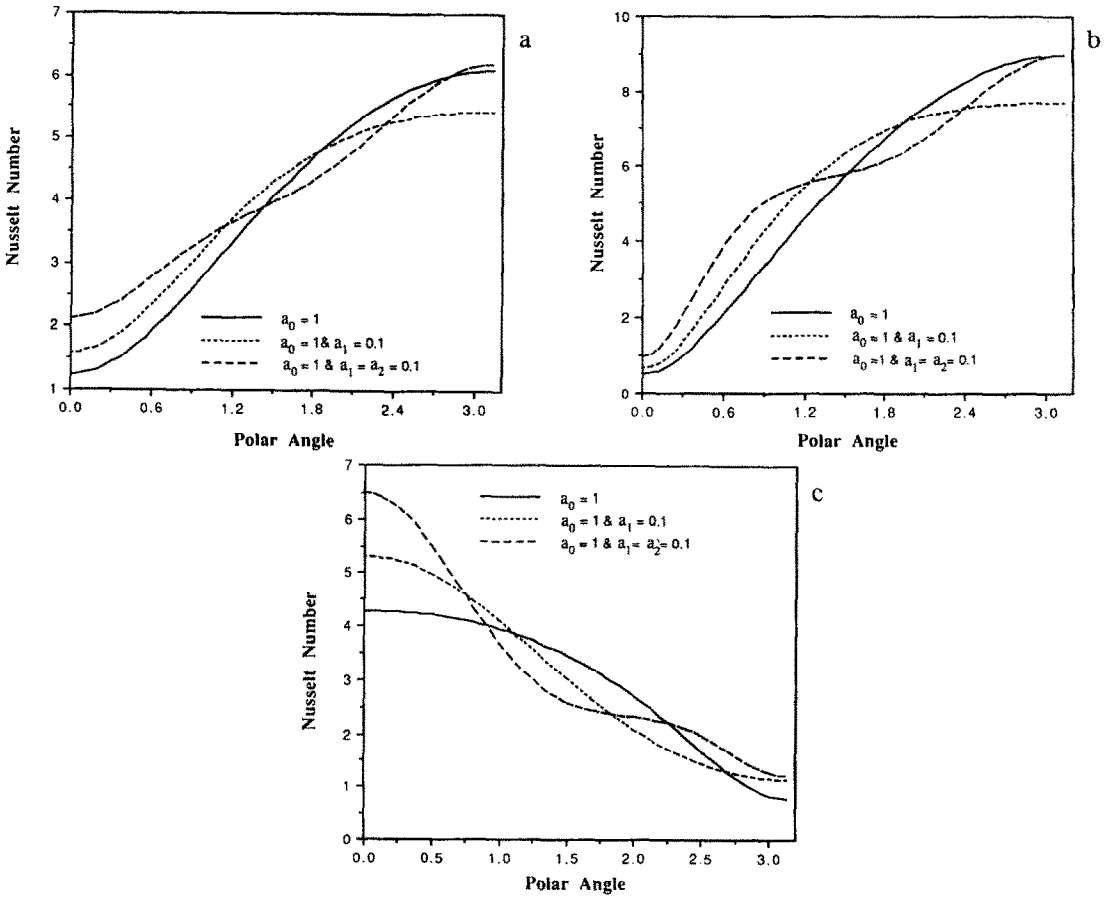

FIG. 6. Effects of surface temperature nonuniformity on local heat flux for $Pe = 10$ with (a) $B = 0$, (b) $B = 10$, (c) $B = -10$.

To examine the role of surface temperature nonuniformity on the heat transfer rate, Fig. 6 shows the local heat flux along the sphere periphery for three cases corresponding to those presented in Figs. 2–4 using three different surface temperature profiles. Clearly, the local heat flux is sensitive to the surface temperature which is not surprising because of their direct relationship. Thus, any perturbation in the surface temperature is also reflected in the local heat flux regardless of the type of convection involved. One interesting point is that with buoyancy opposing the external motion, heat transfer is less intense in the frontal surface than in the rear, which is in contrast to the former cases. Also worthwhile to remark is the overall heat transfer rate which does not seem to be influenced much for all the surface temperature profiles examined, as indicated by small deviations among the areas under those curves. In an effort to assess the overall performance of the heat transfer process, the instantaneous mean Nusselt number is plotted as a function of time in Fig. 7. For $Pe = 10$ and 30 (Figs. 7(a) and (b), respectively), there is a clear distinction about the effects of the buoyancy force direction. However, as Pe increases, this trend is lost since both directions tend to intensify the heat transfer rate as demonstrated in Fig. 7(c) for $Pe = 100$.

It is appropriate at this point to quantitatively validate the results reported above. Though a direct comparison is not possible, there exists a few limiting conditions under which numerical and/or approximate analytical solutions are available [4]. For forced convection, $B = 0$, boundary layer theory predicted the averaged Nusselt number to be

$$Nu = 1.128\sqrt{(Pe)},$$

which is used to compare against our results summarized in Table 2. At a first glance, significant discrepancies, up to 50%, appear to occur at low Peclet number as one would anticipate but the agreement is seen to improve steadily as the Peclet number increases. This finding is expected because boundary-layer approximations are known to be valid only at high Peclet numbers. One apparent fault of the above Nusselt expression is its failure to approach the conduction limit of 2 as Pe goes to zero. Nevertheless, it is a useful correlation for checking the asymptotic behaviors of the numerical solution. For natural convection, one can easily show that the present for-

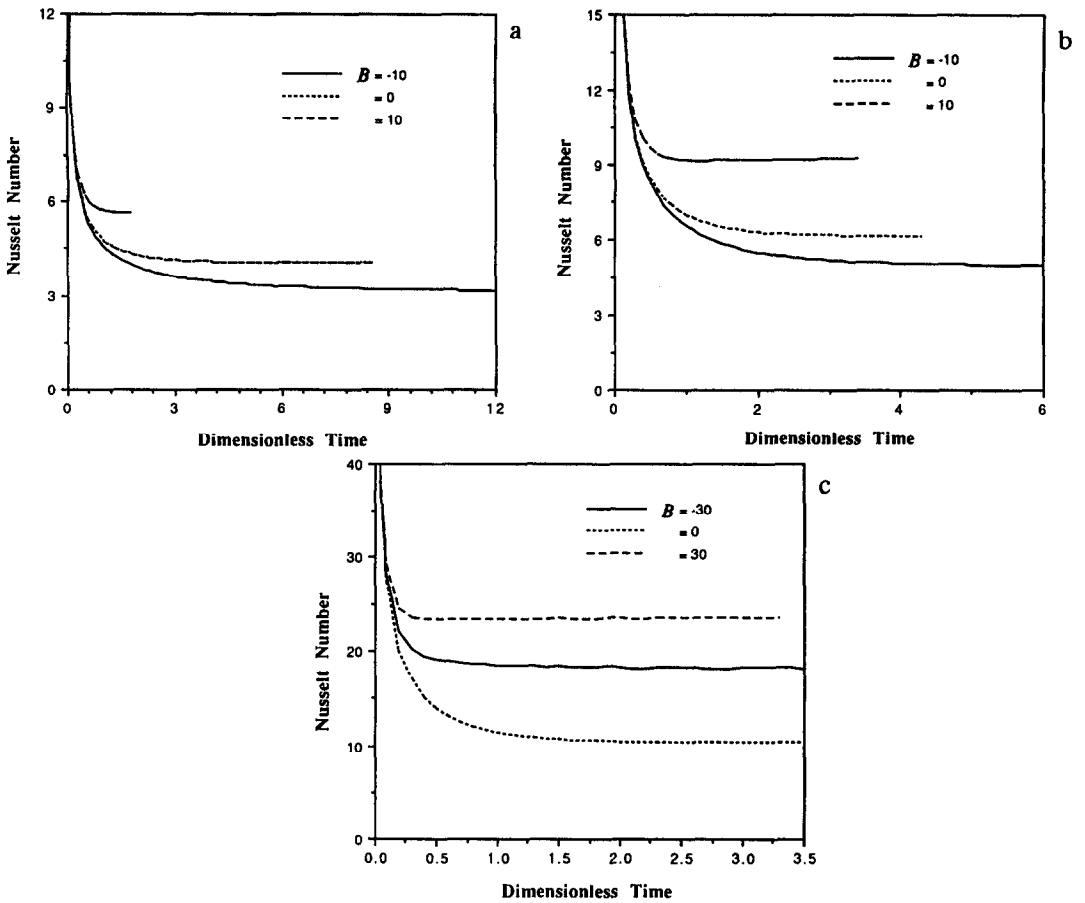

FIG. 7. Time variations of mean Nusselt number with (a) $Pe = 10$, (b) $Pe = 30$, (c) $Pe = 100$.

Table 2. Comparison of steady-state Nusselt numbers in forced convection ($B = 0$)

	$\Phi = 1$	
Pe	Present	Boundary layer [3]
1	2.441	1.128
10	4.570	3.567
50	8.889	7.976
100	12.174	11.280
150	14.703	13.813
200	16.835	15.952

Table 3. Comparison of steady-state Nusselt numbers in natural convection ($U_\infty = 0$)†

	$(B, \Phi) = (1, 1)$		
Pe‡	Present	Ref. [4]	Ref. [3]
10	4.1398	5.6966	3.2378
20	5.5304	6.5468	4.5790
40	7.4856	7.8482	6.4757
70	9.8008	10.0060	8.5665
100	11.534	11.7022	10.2389
150	13.896	14.0680	12.5400
200	15.872	16.4908	14.4800

†Based on linear density–temperature relationship.
‡Pe here is equivalent to $2Ra$ as defined in Pop and Ingham [4].

mulation reduces to that of natural convection in the limit as the free stream velocity approaches zero. In fact, by reassigning the dimensionless quantities ($Pe/2 \to Ra$, $\Phi \to 1$, and $B \to 1$), our governing equations are identical to those of Pop and Ingham [4] who obtained the solutions using a finite differencing scheme. Thus, it is desirable to check our simulation results under those conditions. Table 3 displays a comparison of our data along with the predictions by Pop and Ingham [4] and by boundary layer theory [3]. Once again, one immediately notices substantial discrepancies, ranging from 10% for Ra on the order of a few hundreds to as high as 80% for $Ra \sim 1$, between the numerical results and the boundary layer solutions. Although the disagreement between ours and those of Pop and Ingham [4] is somewhat less serious, it raises a concern because of the unexpectedly large deviations. More importantly, it does not give any indication whether or not the present results are correct. As an attempt to provide more confidence, Table 4 compares the Nusselt numbers for the case of creeping flow past a sphere with $\phi = 1$. Excellent

Table 4. Comparison of steady-state Nusselt numbers for creeping flow past a solid sphere with $\phi = 1$

Pe	Present	Ref. [13]
0	2.000	2.0000
1	2.339	2.2599
10	3.264	3.2240
50	4.697	4.7084
100	5.630	5.6570
200	6.810	6.8578

agreements are obvious as revealed by values which generally differ no more than 4%. It should be pointed out that the data used in the comparison were computed from a correlation which has been known to be accurate to within 2% error [13].

5.2. *Nonuniform heating*

Much of the discussion in the preceeding subsection is speculated to be true for nonuniform heating. To substantiate this claim, we shall again simulate one of the scenarios used previously. In particular, we choose the physical system with $Pe = 10$ and $B = -10$ because of its merit of providing good physical insight. With the uniform surface heat flux ($a_0 = 1$), recirculation zones are delayed to a later time and the size of the recirculation zone is much smaller (see Fig. 8). Moreover, they tend to be confined in the aft portion of the sphere surface rather than expanding throughout the entire surface area in a nearly symmetrical manner as in the previous case. Since the recirculation zone is relatively small, the temperature field is expected to be minimally affected. Indeed, it is very much the same as for the thermally assisted convection case. In order to quantify the effects due to nonuniform heating, Fig. 9 shows the surface temperature at $t = 10$ for three different heat flux profiles: $a_0 = 1$, $a_0 = 1$ and $a_1 = 0.1$, and $a_0 = 1$ and $a_1 = a_2 = 0.1$. It is quite striking that all three surface temperature curves behave in a similar fashion without an inflection point.

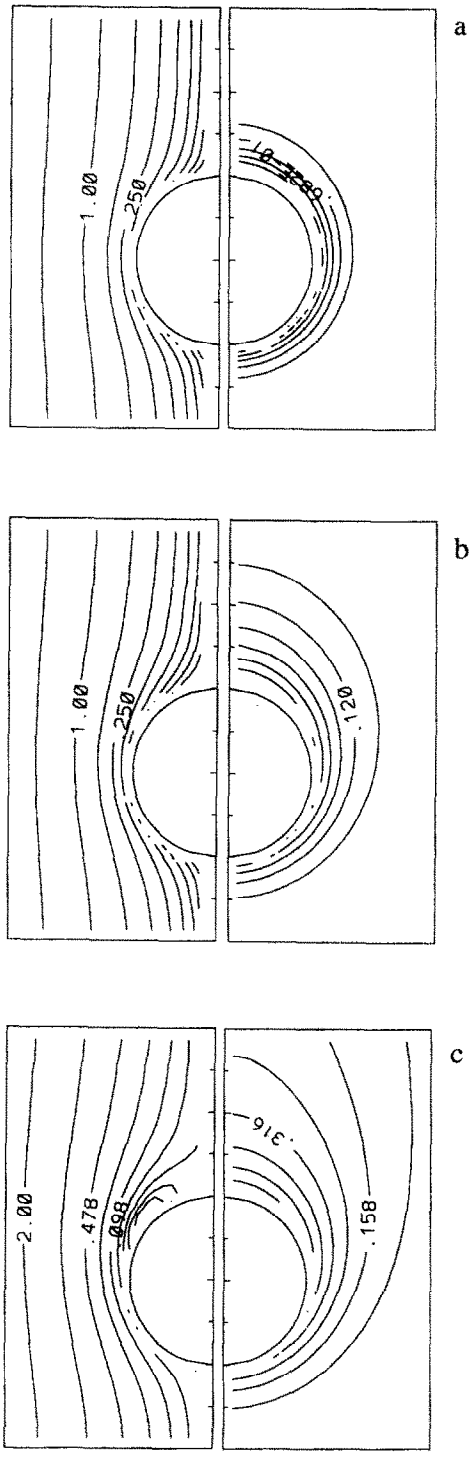

FIG. 8. Streamlines and isotherms for $Pe = 10$, $B = -10$. (a) $t = 0.5$, (b) $t = 2$, (c) $t = 10$.

6. CONCLUDING REMARKS

Heat transfer associated with a sphere embedded in water-saturated porous media and in the presence of forced and natural convection with effects of density inversion is investigated for the cases of variable surface temperature and heat flux. The following conclusions are drawn.

1. For systems with the gravity pointing in the opposite direction to the free stream velocity, the flow in the region near the sphere surface is significantly enhanced by the buoyancy force.

2. When the gravity and the free stream velocity are in the same directions, recirculation zones appear due to counter current flows of the external and the thermally generated motions.

3. The surface heat flux is sensitive to the surface temperature and appears to control the heat flux distribution, but the overall heat transfer rate does not seem to be effected substantially.

4. The non-uniformity in surface heat flux does not alter the shape of the surface temperature profile significantly due to the insensitiveness of the flow under this circumstance.

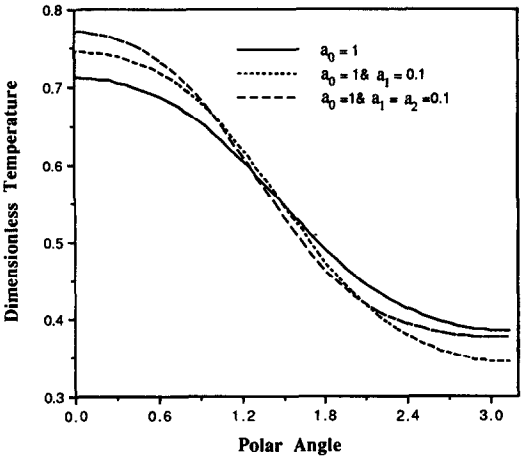

FIG. 9. Surface temperature at $t = 10$.

Acknowledgements—The authors are thankful to Dr R. W. Douglass of the Computational Fluid Dynamics Team of EG&G Idaho, Inc. for his careful reading of the manuscript. This work was performed under the auspices of the U.S. Department of Energy, contract DE-AC07-76-ID01570, and was supported by the INEL Long-Term Research Initiative Program in Computational Mechanics.

REFERENCES

1. C. L. Tien and K. Vafai, Convective and radiative heat transfer in porous media, *Adv. Appl. Mech.* **27**, 225–281 (1990).
2. H. I. Ene and D. Polisevski, *Thermal Flow in Porous Media*. Reidel, Dordrecht (1987).
3. D. A. Nield and A Bejan, *Convection in Porous Media*. Springler, New York (1992).
4. I. Pop and D. B. Ingham, Natural convection about a heated sphere in a porous medium, *Heat Transfer* 1990 **2**, 567–572 (1990).
5. W. J. Minkowycz, P. Cheng and C. H. Chang, Mixed convection about a nonisothermal cylinder and sphere in a porous medium, *Numer. Heat Transfer* **8**, 349–359 (1985).
6. P. Cheng, Mixed convection about a horizontal cylinder and sphere in a fluid-saturated porous medium, *Int. J. Heat Mass Transfer* **25**, 1245–1247 (1982).
7. K. R. Blake, A. Bejan and D. Poulikakos, Natural convection near 4°C in water saturated porous layer heated from below, *Int. J. Heat Mass Transfer* **27**, 2355–2364 (1984).
8. J. R. Philip, Free convection in porous cavities near the temperature of maximum density, *PhysicoChemical Hydrodyn.* **10**, 283–294 (1988).
9. H. D. Nguyen, S. Paik and J. N. Chung, Unsteady conjugate heat transfer associated with a translating spherical droplet: a direct numerical simulation, *Numer. Heat Transfer, Part A* **24**, 161–180 (1993).
10. H.-C. Ku and D. Hatziavramidis, Solution of the two-dimensional Navier–Stokes equations by Chebyshev expansion methods, *Comput. Fluids* **13**, 99–113 (1985).
11. M. Rottenberg, R. Bivins, N. Metropolis and J. K. Wooten, *The 3-J and 6-J Symbols*. MIT Press, Cambridge, MA (1959).
12. H. D. Nguyen and J. N. Chung, A Chebyshev–Legendre spectral method for the transient solution of flow past a solid sphere, *J. Comput. Phys.* **104**, 303–312 (1993).
13. R. Clift, J. R. Grace and M. E. Weber, *Bubbles, Drops, and Particles*, Chap. 3. Academic Press, New York (1978).